Excitonic effects in the optical properties of a SiC sheet and nanotubes

H. C. Hsueh,[1,*] G. Y. Guo,[2,3,†] and Steven G. Louie[4,5]

[1]*Department of Physics, Tamkang University, Tamsui, Taipei 25137, Taiwan*
[2]*Graduate Institute of Applied Physics, National Chengchi University, Taipei 11605, Taiwan*
[3]*Department of Physics, National Taiwan University, Taipei 10617, Taiwan*
[4]*Department of Physics, University of California at Berkeley, Berkeley, California 94720, USA*
[5]*Materials Sciences Division, Lawrence Berkeley National Laboratory, Berkeley, California 94720, USA*

The quasiparticle band structure and optical properties of single-walled zigzag and armchair SiC nanotubes (SiC-NTs) as well as a single SiC sheet are investigated by *ab initio* many-body calculations using the GW and the GW plus Bethe-Salpeter equation approaches, respectively. Significant GW quasiparticle corrections, of more than 1.0 eV, to the Kohn-Sham band gaps from the local density approximation (LDA) calculations are found. The GW self-energy corrections transform the SiC sheet from an indirect LDA band gap to a direct band gap material. Furthermore, the quasiparticle band gaps of SiC-NTs with different chiralities behave very differently as a function of tube diameter, and this can be attributed to the difference in the curvature-induced orbital rehybridization among the different chiral nanotubes. The calculated optical absorption spectra are dominated by discrete exciton peaks due to exciton states with a high binding energy, up to 2.0 eV, in the SiC sheet and SiC-NTs. The formation of strongly bound excitons is attributed to the enhanced electron-hole interaction in these low-dimensional systems. Remarkably, the excited electron amplitude of the exciton wave function is found to peak on Si atoms near the hole position (which is on the C site) in zigzag SiC-NTs, indicating a charge transfer from an anion (hole) to its neighboring cations by photoexcitation. In contrast, this pronounced peak structure disappears in the exciton wave function in armchair SiC-NTs. Furthermore, in armchair SiC-NTs, the bound exciton wave functions are more localized and also strongly cylindrically asymmetric. The high excitation energy, ~3.0 eV, of the first bright exciton, with no dark exciton below it, suggests that small-radius armchair SiC-NTs could be useful for optical devices working in the UV regime. On the other hand, zigzag SiC-NTs have many dark excitons below the first bright exciton and hence may have potential applications in tunable optoelectric devices ranging from infrared to UV frequencies by external perturbations.

PACS number(s): 81.07.De, 73.22.−f, 78.67.Ch, 73.63.Fg

I. INTRODUCTION

Silicon carbide (SiC) crystallizes in either a cubic or a hexagonal form and exbihits interesting polytypism.[1,2] The polytypes are made of identical hexagonal layers with different stacking sequences. These polytypes are semiconductors with a range of band gaps, from 2.39 eV in the zincblende polytype (3C) to 3.33 eV in the wurtzite polytype (2H).[1,3] Furthermore, 3C and 6H SiC are used for high-temperature, high-power, and high-frequency devices[4–7] due to their unique properties,[8] while 6H SiC, with a band gap of 2.86 eV, is a useful material for blue-light-emitting diode applications.[3]

Recently, SiC nanotubes (NTs) were synthesized by reaction of carbon nanotubes (CNTs) with SiO at various temperatures.[9] Like other tubular materials, such as C,[10–12] BN,[13,14] AlN,[15] and GaN[16] NTs, that have been synthesized previously, SiC-NTs display very interesting properties distinctly different from those of their bulks. Therefore, the successful synthesis of SiC-NTs has stimulated a number of theoretical and experimental investigations on the tubular form of SiC (see Refs. 17 and 18 and references therein). In particular, based on density functional calculations, Miyamoto and Yu[19] predicted that the strain energies of SiC-NTs are lower than those of CNTs and that the band gaps of SiC-NTs can be direct or indirect, depending on the chirality. Using both tight-binding molecular dynamics and *ab initio* methods, Menon and coworkers[20] showed that single-walled SiC-NTs are very stable, with a large band gap.

Unlike CNTs, SiC-NTs are polar materials and, therefore, may exhibit unusual physical properties that CNTs may not have. For example, like BN-NTs (see, e.g., Refs. 21 and 22), zigzag SiC-NTs may become piezoelectric and, also, show second-order nonlinear optical response. Knowledge of the optical properties of SiC-NTs is important for their optical and electro-optical applications. Therefore, Wu and Guo have recently carried out a series of *ab initio* calculations within the density functional theory (DFT) with the local density approximation (LDA) in order to analyze the linear optical features and underlying band structure as well as the second-harmonic generation and linear electro-optical coefficients of all three types of the SiC-NTs.[17,18] In particular, Wu and Guo found that all the SiC NTs are semiconductors with the exceptions of the ultrasmall (3,0) and (4,0) zigzag tubes, which may be regarded as the thinnest conducting SiC nanowires.[17] Interestingly, the band gap of the zigzag SiC-NTs may be reduced from the energy gap of the SiC sheet all the way down to 0 by reducing the diameter, though the band gap for all SiC NTs with a diameter larger than ~20 Å approaches that of the SiC sheet. Furthermore, DFT indicates that all semiconducting *zigzag* SiC-NTs have a direct band gap. All these suggest that they may have interesting applications in optical and optoelectronic devices. Nonetheless, both armchair and chiral SiC-NTs have an indirect band gap at the DFT level.

These previous theoretical studies of the electronic and optical properties of SiC-NTs were based on the independent-

particle approximation within the DFT framework[17,18] or on semiempirical calculations.[20] However, many-body interactions are known to play an important role in low-dimensional systems such as NTs,[23,24] due to reduced charge screening and enhanced electron-electron correlation. Therefore, motivated by the prospects of optoelectronic device applications of SiC-NTs and also this theoretical issue, we have performed *ab initio* calculations to study many-body effects on quasiparticle band gaps and optical spectra of SiC-NTs. Indeed, we find pronounced GW quasiparticle corrections, of more than 1.0 eV, to the LDA band gaps in SiC-NTs. Further, the calculated optical absorption spectra of SiC-NTs are dominated by discrete exciton peaks due to strongly bound excitons with a high binding energy, up to 2.0 eV.

SiC-NTs can be considered an atomic layer of a SiC sheet rolled up into a cylinder, and similarly to the CNTs, the structure of a SiC-NT is specified by the chiral vector, which is given in term of a pair of integers (n,m).[11] Understanding the optical properties of an isolated SiC sheet would help us to understand many-body effects on the optical responses of SiC-NTs. Therefore, a single-atomic-layer hexagonal SiC sheet is considered first here. Furthermore, the optical properties of the two-dimensional (2D) single SiC sheet are interesting on their own account, and, in particular, a single SiC sheet bears many similarities to graphene, which exhibits many fascinating properties.[25,26]

This paper is organized as follows. In the next section, the theoretical methods and computational details, including the ground-state, quasiparticle, and electron-hole interaction calculations, are described. In Sec. III, the calculated quasiparticle band structure and optical absorption spectra of the isolated SiC sheet are presented. In Sec. IV, the calculated quasiparticle band structures of SiC-NTs are reported and the effects of curvature and chirality on the band gaps are analyzed. In Sec. V, the calculated optical absorption spectra of the SiC-NTs are presented, and the excitonic effects are discussed. Finally, the conclusions drawn from this work are given in Sec. VI.

II. METHODOLOGY

In the present paper, we adopt the approach of Rohlfing and Louie[27,28] and hence calculate the quasiparticle energies, electron-hole excitations, and optical spectra from first principles in three steps. First, we calculate the electronic ground state with DFT in the LDA.[29] Second, we obtain the quasiparticle energies (E^{QP}) within the GW approximation for the electron self-energy Σ.[30,31] Finally, we evaluate the coupled electron-hole excitation energies and optical spectra by solving the Bethe-Salpeter equation (BSE) of the two-particle Green's function.[27,28] Details of our computations are described below.

A. Ground-state properties

An appropriate mean-field description of the ground-state properties of solids is essential to perform quasiparticle calculations within many-body perturbation theory. For conventional covalent and ionic bonded materials, it is shown[31] that eigen–wave functions and eigenenergies of the Kohn-

Sham equation[29] in the LDA provide a good starting point for many-body perturbation calculations such as within GW approximations. Therefore, in this paper, the ground-state electronic structure of the single SiC sheet and SiC-NTs are first calculated by means of the *ab initio* plane-wave pseudopotential method.[32] The electronic configurations of $Si(3s^2, 3p^2)$ and $C(2s^2, 2p^2)$ are treated as active valence states when generating pseudopotentials in the Kleinman-Bylander form[33] for all calculations. The cutoff energy of 40 Ry is used for the plane-wave basis set. Also, to ensure convergency, the Brillouin-zone (BZ) integrals for calculations of the SiC sheet and SiC-NTs are carried out using $10 \times 10 \times 1$ and $1 \times 1 \times 32$ Monkhorst-Pack k-grid sampling,[34] respectively. The supercell approach is used here, such that an isolated SiC sheet (NT) is approximated by a single SiC layer (NT) surrounded by a vacuum in a supercell. Sufficient intersheet and intertube separations (more than 10 Å) are used to prevent intersheet and intertube interactions. The underlying atomic positions and lattice constants are taken from Ref. 17, where the theoretical structures were obtained by the conjugate gradient method, with the atomic forces and the stress calculated from first principles.

B. Quasiparticle calculations

Based on the ground-state Kohn-Sham wave functions and corresponding eigenvalues (E^{KS}) calculated above, many-body effects on the quasiparticle band structure characterized by the self-energy (Σ) can be evaluated by solving the Dyson equation,[30,31,35]

$$\left[H_0 + \Sigma\left(E_{n\mathbf{k}}^{\mathrm{QP}}\right)\right]|n\mathbf{k}\rangle = E_{n\mathbf{k}}^{\mathrm{QP}}|n\mathbf{k}\rangle, \tag{1}$$

where H_0 is the Hamiltonian in the Hartree approximation, and $|n\mathbf{k}\rangle$ represents the quasiparticle wave function of energy $E_{n\mathbf{k}}^{\mathrm{QP}}$ within the one-particle Green's function method. In the G^0W^0 approximation, the vertex correction is approximated by a δ function and the irreducible polarizibility P^0 is a convolution of the mean-field Green's function G^0, i.e., $P^0 = -iG^0G^0$. This gives rise to a dynamical dielectric matrix within the random phase approximation (RPA) scheme and a generalized plasmon-pole model.[31] Also, the screened Coulomb potential W^0 can be obtained from the bare Coulomb interaction v through the equation $W^0 = v/[1 - vP^0]$. Finally, the quasiparticle self-energy operator is given by $\Sigma = iG^0W^0$. Although alternatives have been proposed recently to calculate the self-energy going beyond this approximation, the G^0W^0 approach is still the most efficient scheme for providing a successful description of the electronic excitation and even transport properties in various semiconductors, metals, surfaces, and novel nanomaterials.[36–38] Therefore, in this paper, we adopt the G^0W^0 approach to calculate the quasiparticle properties of a single SiC sheet and SiC-NTs. Here a rather dense k-point sampling for the SiC sheet ($18 \times 18 \times 1$) and also for the SiC-NTs ($1 \times 1 \times 32$) is used to ensure that the calculated quasiparticle energies converge to within 0.05 eV.

A proper description of the dynamical screening properties of a solid plays an important role in obtaining its quasiparticle properties reliably. In low-dimensional systems, this requirement becomes crucial due to the highly anisotropic screening interactions associated mainly with the vacuum
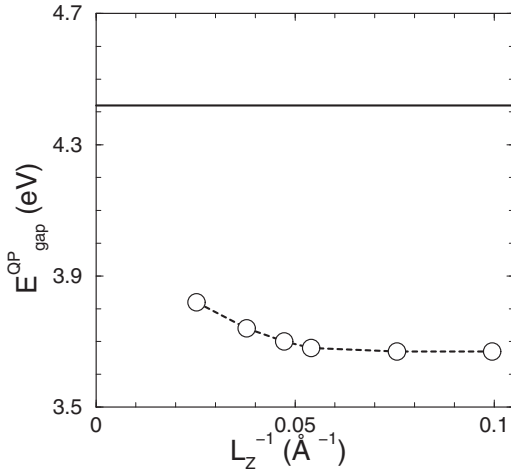
FIG. 1. Calculated quasiparticle band gap of a SiC sheet (open symbols) as a function of the inverse of the intersheet separation (L_z). The converged band gap, indicated by the solid line, is derived by employing the Coulomb truncation scheme. The dashed line linking the open circles is a guide for the eye only.

region between the isolated units in the supercell scheme. A larger vacuum region is preferred to reduce the residual unphysical interunit interaction and eventually end up with an ideal vacuum screening of the isolated units. For example, the band gap of an isolated SiC sheet, as shown in Fig. 1, would increase as the screening from neighboring layers is reduced by increasing the separation (L_z) between the SiC layers in the neighboring supercells. Furthermore, the convergence of the band gap with respect to the spatial separation of the neighboring SiC layers is very slow. Due to the computation constraints, it is impossible to obtain the fully converged band gap simply by expanding the interlayer separation. Therefore, an efficient truncation scheme[39,40] for the Coulomb interaction in which a step function at the boundary of the supercell is introduced will be adopted in the present GW and BSE calculations to remove the long-range Coulomb interaction between the structure and its images. Figure 1 clearly demonstrates that the truncation scheme indeed offers an efficient means to achieve a converged quasiparticle band gap for low-dimensional structures. Table I further shows that the quasiparticle band gap and also quasiparticle energy differences from the GW calculations with or without the Coulomb truncation scheme can differ significantly.

TABLE I. Band gap (E_{gap}) and quasiparticle energy differences between the conduction band minimum (c) and the valence band maximum (v) at some high-symmetry k points of a SiC sheet from the LDA and GW calculations [without (no trunc.) and with (trunc.) the Coulomb truncation]. All energies are given in electron volts.

	LDA	GW	
	No trunc.	No trunc.	Trunc.
E_{gap}	2.51	3.66	4.42
$K^v \rightarrow K^c$	2.56	3.66	4.42
$\Gamma^v \rightarrow \Gamma^c$	4.46	5.58	6.04
$M^v \rightarrow M^c$	3.23	4.60	5.40

C. Electron-hole excitations

The optical properties of a solid, associated with the interaction between light and the electronic excitations of a system, are described by the frequency-dependent macroscopic dielectric function $\epsilon(\omega)$. For example, the optical absorption spectrum is determined by the imaginary part of the dielectric function, $\epsilon_2(\omega)$. According to the Fermi Golden Rule, the transition energy associated with a peak in the optical absorption spectrum can be estimated from the energy difference between the associated electron and hole states. The corresponding oscillator strength can be obtained from the optical transition matrix elements derived from the electronic ground and excited states involved. Since the incident photons carry negligible momentum, the peaks in the optical absorption spectrum can be considered direct interband transitions between occupied and unoccupied electronic states without any crystal momentum transfer. Therefore, ignoring the electron-hole interaction, both linear and nonlinear optical spectra can be calculated in an independent-particle approximation by including only the vertical interband transitions between the Kohn-Sham states.[17,18] In the GW + RPA approach, the dielectric function calculated based on the quasiparticle energies, as described above, gives the interband optical absorption spectrum beyond the LDA but still without electron-hole interaction (or excitonic) effects.

However, for systems with strong excitonic effects, the optical properties may be dominated by excitons which are composed of strongly correlated electron-hole pairs of the systems. The connection of the exciton energies Ω^S and corresponding electron-hole amplitudes A_{vck}^S of the correlated electron-hole excitations S is governed by the BSE,[28]

$$(E_{c\mathbf{k}} - E_{v\mathbf{k}})A_{vc\mathbf{k}}^S + \sum_{v'c'\mathbf{k}'}\langle vc\mathbf{k}|K^{ph}|v'c'\mathbf{k}'\rangle A_{vc\mathbf{k}}^S = \Omega^S A_{vc\mathbf{k}}^S,$$

(2)

where $E_{v\mathbf{k}}$ ($E_{c\mathbf{k}}$) denotes the quasiparticle (e.g., GW) eigenvalues of valence (conduction) bands at a specific $\mathbf{k}$ point and K^{eh} is the kernel describing the interaction between excited electrons and holes. Therefore, a more realistic two-particle picture of optical excitations including excitonic effects in these systems should be provided by means of the GW + BSE method. To obtain converged optical spectra, in the present work, the kernel K^{eh} of the SiC sheet (SiC-NTs) is computed on a sparse k-point grid of $18 \times 18 \times 1$ ($1 \times 1 \times 32$) and then interpolated[27] onto a denser k-point grid of $36 \times 36 \times 1$ ($1 \times 1 \times 64$).

Instructively, the electron-hole amplitude in real space can be expanded in the quasielectron and quasihole basis $\{\phi_{c\mathbf{k}}(\mathbf{r}_e), \phi_{v\mathbf{k}}(\mathbf{r}_h)\}$,

$$\Phi_S(\mathbf{r}_e, \mathbf{r}_h) = \sum_{\mathbf{k}}\sum_{c,v} A_{vc\mathbf{k}}^S \phi_{c\mathbf{k}}(\mathbf{r}_e)\phi_{v\mathbf{k}}(\mathbf{r}_h),$$

(3)

and the corresponding exciton states can be visualized in real space. Because of the complexity of the six-dimensional exciton wave function, a simpler distribution of the electron amplitude square with the hole position fixed, i.e., $|\Phi_S(\mathbf{r}_e, \mathbf{r}_h = 0)|^2$, is usually used to reveal the essence of the electron-hole correlation of the exciton.[23,24]

Finally, as noted before,[12,17] the employment of a 3D supercell method for reduced-dimensional systems will generate an

arbitrary volume effect on the dielectric function computation. In order to resolve this ambiguity and make direct comparisons to experimental measurements, we calculate the imaginary part of the polarizability per unit area (in units of nm) for a SiC sheet, $\alpha_2(\omega)$, which is derived from the calculated dielectric susceptibility, $\chi = (\epsilon - 1)/4\pi$, multiplied by the distance between two neighboring SiC sheets.[41] Moreover, for 1D NTs, the measured optical spectrum is determined by the imaginary part of the optical polarizability per single tube, $\alpha_2(\omega)$. This α_2 is equal to the ϵ_2^{calc} multiplied by the cross-sectional area of the supercell perpendicular to the tubular axis ($\Lambda_{\text{sc}}^\perp$), i.e., $\alpha_2 = \Lambda_{\text{sc}}^\perp(\epsilon_2^{\text{calc}})/4\pi$.

III. ELECTRONIC AND OPTICAL PROPERTIES OF THE SILICON CARBIDE SHEET

In recent DFT-LDA calculations, a stable, nonbuckled graphene-like monolayer has been found for an isolated SiC layer.[17,42] Despite the structural similarity, the unique massless Dirac fermion feature in graphene is no longer present in the SiC sheet because of the different ionicities of the Si and C atoms. This heteropolar character induces an energy gap of 2.56 eV (the LDA value) at the k point of the hexagonal Brillouin zone, as shown in Fig. 2. The quasiparticle corrections to the 2D SiC sheet state are obtained through the GW calculations described above. The calculated quasiparticle band gaps and energy differenes at some high-symmetry k points are summarized in Table I. It is clear from Table I that the GW corrections to the LDA eigenvalues are rather significant, being more than 1.0 eV. We note that the GW correction to the LDA band gap of bulk 2H SiC is around 1.0 eV.[43,44] Strikingly, the GW corrections transform the indirect LDA band gap ($K \rightarrow M$) into a direct band gap ($K \rightarrow K$) for the SiC sheet. The nature of the direct band gap in the 2D SiC sheet indicates that the lowest energy exciton in the SiC sheet is optically active (bright). Furthermore, based on the simple zone-folding approximation, we would expect no momentum-mismatch-induced optically inactive (dark) excitons below the lowest energy bright exciton in the SiC-NTs.[45] This anticipation is indeed confirmed by our GW + BSE calculations for both the SiC sheet and the armchair SiC-NTs presented below. However, our GW + BSE calculations also show that this is not the case for very small zigzag SiC-NTs, as discussed in Sec. V.

Figure 2 shows the LDA band structure (left) and also the GW corrections to the LDA eigenvalues (right) of the 2D SiC sheet. We note that the optical dielectric function of the 2D SiC sheet is highly anisotropic (see, e.g., Ref. 17). In particular, there is only weak dynamical screening for the electric field perpendicular to the sheet in the energy range below 6 eV, whereas the dynamical screening for the in-plane electric field is strong in this energy range (see Fig. 1 in Ref. 17). Therefore, many-body interaction effects in the π band (red line in Fig. 2) associated with the p_z orbitals, which extend into the vacuum region from the sheet, would be less screened. Consequently, the π band would have a larger quasiparticle correction and hence have a larger difference between the quasiparticle energies and the LDA eigenvalues ($E^{\text{QP}} - E^{\text{LDA}}$) [(red) circles in Fig. 2]. On the other hand, because the in-plane σ bonds are mainly confined to the 2D SiC sheet, electric
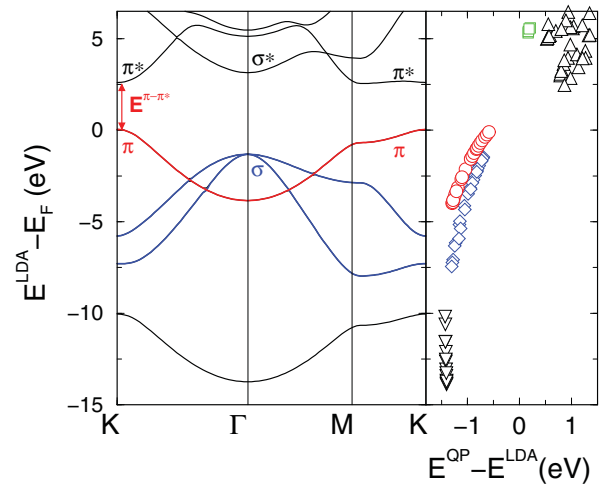

FIG. 2. (Color online) LDA band structure (left panel) and GW corrections to LDA eigenvalues (right panel) of the graphitic SiC sheet. Left: The π and σ bands are shown as red and blue lines, respectively. The LDA $E^{\pi-\pi*}$ gap is shown by the arrow. The valence band maximum is aligned at 0 eV. Right: GW corrections for the π and σ bands are represented by red circles and blue diamonds, respectively, whereas GW corrections of the NFE states are represented by green squares.

screening effects on the σ bands (blue lines in Fig. 2) are more significant, and hence GW corrections are smaller [(blue) diamonds in Fig. 2]. Furthermore, due to weak many-body interactions in nearly free electron (NFE) states, which mainly lie more than a few angstroms above and below the SiC sheet, the GW corrections to these conduction bands are small, being less than 0.3 eV [(green) squares in Fig. 2]. This is similar to the NFE states in graphene.[47] These sophisticated screening effects enforce the notion that quasiparticle calculations rather than simple scissor-operator approximations are necessary for low-dimensional systems such as a 2D SiC sheet.

Excitonic effects on the optical properties of the SiC sheet can be examined by comparing the GW + RPA results with the GW + BSE calculations. Because of the huge depolarization effect in the 2D planar geometry for light polarization perpendicular to the plane, we focus on the optical absorption spectrum for light polarization parallel to the plane. Figure 3 shows the optical spectra of (a) both the GW + RPA and the GW + BSE calculations and (b) the $E_1^{\pi-\pi*}$ exciton wave function of the SiC sheet. In Fig. 3(a), the first prominent peak, located at $E_1^{\pi-\pi*} = 3.25$ eV, in the GW + BSE absorption spectrum comes from a bright exciton due to the excitation between the π and the $\pi*$ states at the K point [see Fig. 2 (left)]. This is a strongly bound exciton with the high binding energy of $E_1^{\text{Bind}} = 1.17$ eV as measured by the difference between the $E_1^{\pi-\pi*}$ and the onset energy of the GW corrected electron-hole continuum ($E^{\pi-\pi*} = 4.42$ eV). We note that the theoretical exciton binding energy in bulk 2H SiC is only 0.1 eV.[44] This shows clearly that the reduced dimensionality of a SiC sheet strongly confines the quasiparticles, and this significantly enhances the overlap between the electron and the hole wave functions and hence the electron-hole interaction. In addition to this quantum confinement, the presence of the vacuum region reduces the screening and hence provides an
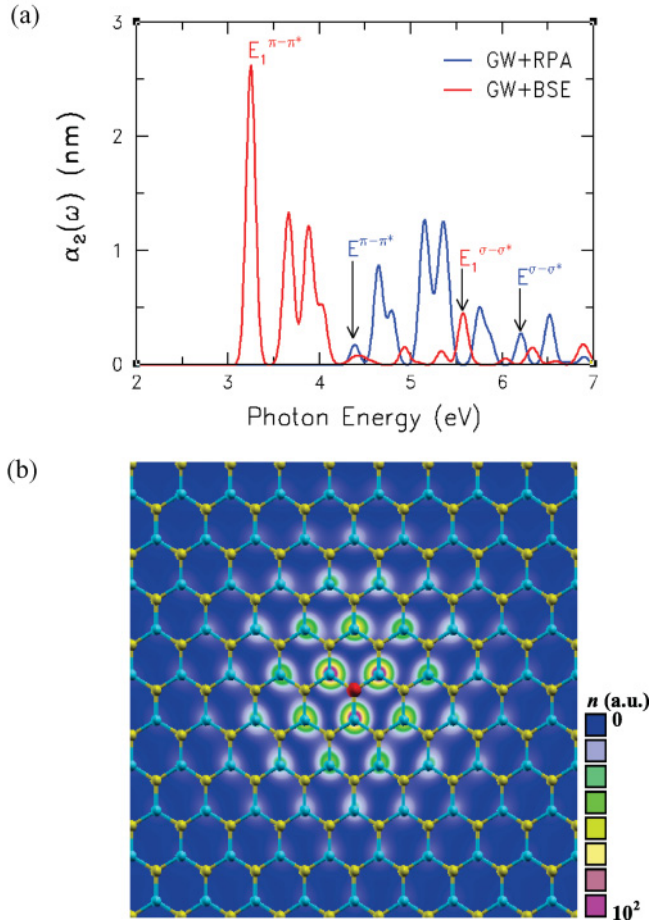
FIG. 3. (Color online) (a) Optical polarizability per unit area from both GW + RPA (blue line) and GW + BSE (red line) calculations and (b) $E_1^{\pi-\pi*}$ exciton wave function of the SiC sheet. (a) Theoretical spectra are broadened with a Gaussian smearing width of 0.15 eV. (b) The hole position (red sphere) is fixed at the top of a C atom (yellow sphere) and the squared electron amplitude [$n = |\Phi_S(\mathbf{r}_e, \mathbf{r}_h = 0)|^2$ in arbitrary units (a.u.)] is mainly distributed on Si atoms (cyan spheres) next to the hole.

extra contribution to the large excitonic effect in the SiC sheet. An analysis of $\int |\Phi_S(\mathbf{r}_e, \mathbf{r}_h)|^2 d\mathbf{r}_e$ and $\int |\Phi_S(\mathbf{r}_e, \mathbf{r}_h)|^2 d\mathbf{r}_h$ shows that the hole resides mainly in the C sublattice, whereas the excited electron is on the Si sublattice. In order to elucidate the extent of the $E_1^{\pi-\pi*}$ exciton wave function, we plot the electron amplitude square with the hole fixed at a position slightly above the C atom [see Fig. 3(b)]. Clearly, the electron orbital is of the p_z character and distributes mainly on the nearest-neighbor Si atoms around the hole to form a fairly localized exciton.

In the optical absorption spectrum of the SiC sheet $\alpha_2(\omega)$ from the GW + BSE calculations, the low-energy features in the energy range from 3.0 to 5.0 eV [Fig. 3(a)] are dominated by $\pi \rightarrow \pi^*$ transitions near the K point at the zone edge (Fig. 2), whereas the pronounced absorption peak at 5.83 eV is mainly due to the $\sigma \rightarrow \sigma^*$ transition at the zone center. As shown in Fig. 3(a), the electron-hole interaction not only triggers a red shift of the onset optical transition energies but also modifies their relative absorption intensities. Furthermore, because the GW corrections transform the indirect LDA band

gap of the SiC sheet into the direct band gap, as mentioned above, no dark exciton was found in the optical spectrum until a photon energy of up to 4.2 eV, which is above the lowest bright exciton ($E_1^{\pi-\pi*}$).

IV. QUASIPARTICLE BAND STRUCTURE OF SILICON CARBIDE NANOTUBES

An intuitive approach to constructing an NT with a specific chirality is simply to roll up a layer of the graphitic sheet along a specific lattice vector into a nanocylinder. This geometrical connection between a single-wall NT and the isolated sheet has inspired the application of the zone-folding method to construction of a zeroth-order electronic band structure and phonon dispersions for single-wall NTs.[11] However, the zone-folding scheme alone cannot address the significant orbital rehybridization due to the curvature effect and also the many-body interaction effects in the NTs mentioned above. To include these effects, we have calculated the diameter dependence of the fundamental quasiparticle band gap of some small-radius zigzag and armchair SiC-NTs, as compiled in Fig. 4. First, we note that all the SiC-NTs are semiconductors, and this may be attributed to the different potentials of Si and C atoms, being similar to the case of BN NTs.[13] Second, an asymptotic convergence of the calculated band gaps of zigzag and armchair SiC-NTs as a function of tube size toward that of the isolated SiC sheet is observed in both LDA and GW calculations.

Interestingly, in contrast to the reciprocal radius dependence of the band gap in CNTs, we find a peculiar band gap reduction with a decrease in tube size for both zigzag and armchair SiC-NTs. This band gap reduction of SiC-NTs with increasing tubular curvature can be attributed to the curvature-induced hybridization between π^* and σ^* orbitals near the conduction band minimum (CBM) in small-radius SiC-NTs, similar to
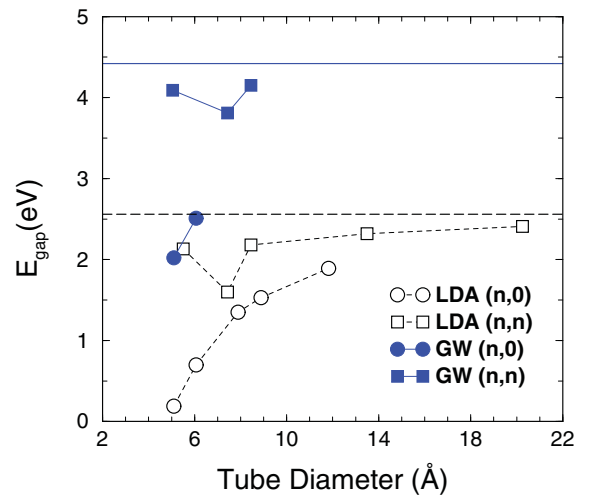

FIG. 4. (Color online) Fundamental band gaps of some zigzag $(n,0)$ and armchair (n,n) SiC nanotubes as a function of the tube diameter from the GW (filled symbols) and LDA[17](open symbols) calculations. The band gap of the isolated SiC sheet obtained from the GW and LDA calculations is also displayed as the solid and the dashed line, respectively. Dotted lines between the symbols are a guide for the eye only.
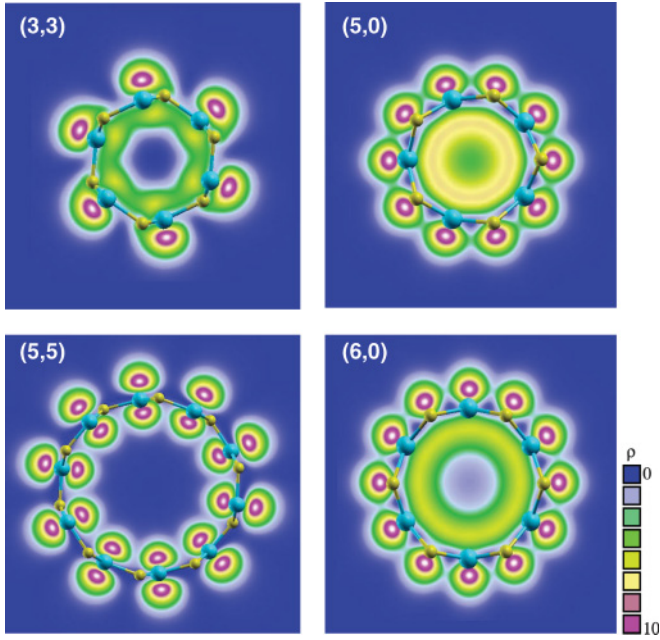
FIG. 5. (Color online) Charge density contours (ρ in 10^{-2} $\mathring{A}^{-3}$) of states at the conduction band minimum (CBM) at the 1D Brillouin zone boundary (Z point) of (3,3) and (5,5) SiC-NTs and also at the zone center (Γ point) of (5,0) and (6,0) SiC-NTs. Si and C atoms are represented by cyan and yellow spheres, respectively.

FIG. 6. Energy differences between the quasiparticle eigenvalues(E^{QP}) and LDA eigenenergies (E^{LDA}) of the armchair (3,3) (upper panel) and zigzag (5,0) (lower panel) SiC-NTs. The corresponding LDA band structures are shown in the left panels for reference. Dashed lines denote the valence band maximum at 0 eV.

that found in the very small diameter CNTs.[46] To illustrate this point, we display the charge density contours of the CBM of the zigzag (n,0) and armchair (n,n) NTs at the 1D Brillouin zone center (Γ point) and zone boundary (Z point), respectively, in Fig. 5. Figure 5 shows that in the small zigzag (n,0) SiC-NTs such as (5,0) and (6,0) NTs, a strong mixture of the π^* and σ^* states in the SiC sheet now exists inside the tube to form a ring-like charge distribution, whereas the feature of the p_z state is floating above the Si and C atoms outside the SiC-NT even under considerable structural distortion. Therefore, a substantial band gap reduction can be expected upon increasing the tube curvature. Indeed, this is confirmed by our LDA and quasiparticle calculations (see circles in Fig. 4). In contrast, a much smaller degree of orbital hybridization in armchair SiC-NTs is induced by the folding curvature, as revealed by the cylindrically symmetric distribution of the Si p_z component of the CBM at the Brillouin zone boundary (Z point) in the (5,5) NT (Fig. 5). This gives rise to a minor size dependence of the band gap (squares in Fig. 4) for armchair SiC-NTs. Nevertheless, a spectacular curvature effect in terms of strongly enhanced π^*-σ^* hybridization does occur in the ultrasmall armchair (3,3) SiC-NT (see Fig. 5). This unusual orbital rehybridization effect on the band gap has also been recognized before in other ionic group III-V NTs.[14,45]

The quasiparticle corrections to the Kohn-Sham eigenvalues from the GW calculations for two ultrasmall (radius, $\sim$5 Å) armchair (3,3) and zigzag (5,0) SiC-NTs are given in Fig. 6, together with their LDA band structures. In the (3,3) SiC-NT, the GW corrections widen the LDA indirect band gap (2.13 eV) to the direct one of 4.09 eV and, also, modify the band dispersions significantly as a result of the complicated energy dependence of the GW corrections (see open circles in
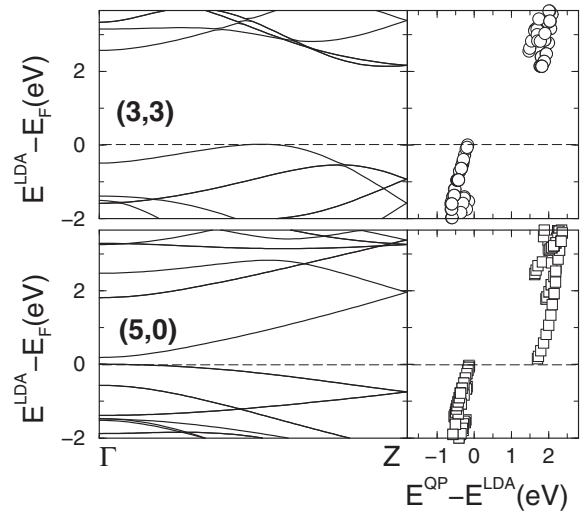
Fig. 6). Meanwhile, the small direct band gap (0.19 eV) of the (5,0) SiC-NT predicted by the LDA is increased to 2.02 eV in the GW calculations. Furthermore, the GW corrections depend rather sensitively on the electronic state character, as illustrated in Fig. 6 for the (5,0) SiC-NT (open squares). We note that the curvature-induced hybridization between the π and the σ states in these ultrasmall SiC-NTs is responsible for the mixture of the quasiparticle corrections of the otherwise orthogonal π and σ states near the top of the valence band in the SiC sheet. This hybridization will become weaker gradually as the tube radius increases and eventually diminishes in the large-tube-radius limit where the self-energy corrections will be the same as those of the SiC sheet (as shown in Fig. 2). The NFE tubular states are found in both (3,3) and (5,0) tubes as well as the small-radius chiral SiC-NTs. However, these NFE states lie in the rather high-energy region (more than 5 eV above the band gap region from LDA calculations) and hence play a minor role in the optical absorption spectrum. Therefore, they are not included in the present GW and GW + BSE calculations. Nonetheless, the NFE states can be shifted downward toward the band gap regime by doping electrons in the NTs[48] and, consequently, may significantly affect the optical properties of n-type SiC-NTs.

V. EXCITONIC EFFECTS IN SILICON CARBIDE NANOTUBES

In quasi-1D NT systems, the wave functions of quasielectrons and quasiholes can overlap significantly because of quantum confinement, and therefore, electron-hole interaction may be considerably enhanced. At the same time, the screening among quasiparticles can be systematically changed because of curvature and reduced-dimensionality effects. For example, the phenomenon of antiscreening was discovered recently in CNTs.[49] Therefore, the absorption features associated with
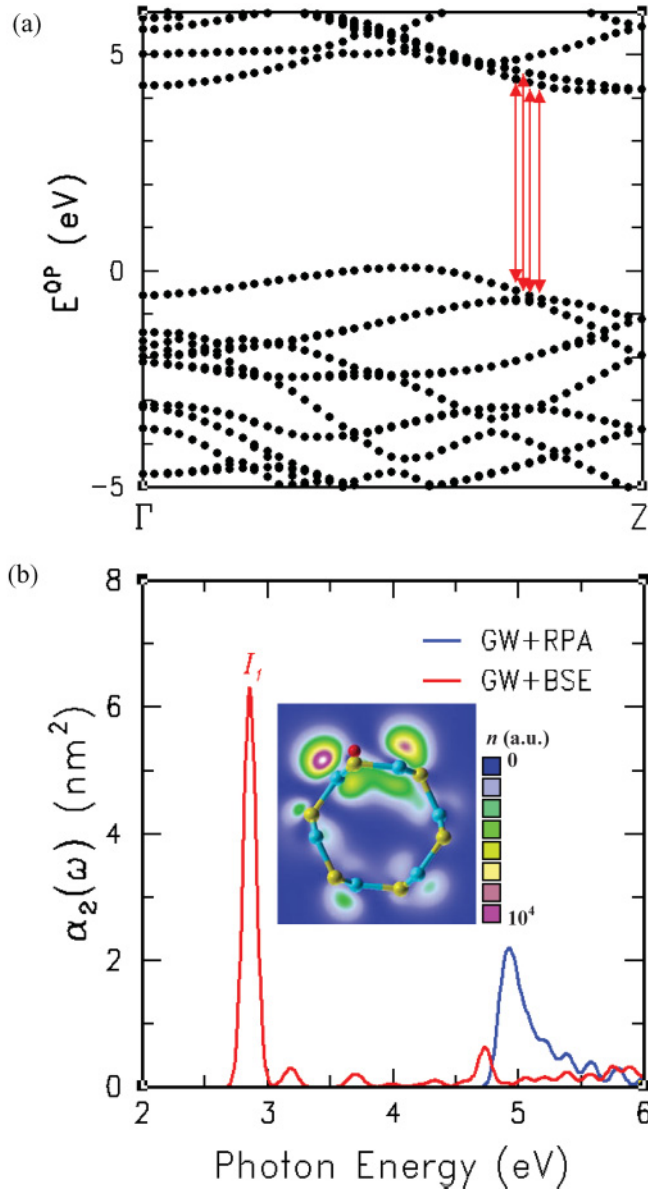
(a)

(b)

FIG. 7. (Color online) (a) Quasiparticle band structure and (b) optical absorption spectra of the armchair (3,3) SiC-NT. (b) Optical spectra from GW + RPA and GW + BSE calculations are shown as the dashed (blue) and solid (red) curves, respectively. Theoretical absorption spectra were broadened with a Gaussian of 0.15 eV. The lowest energy bright exciton (I_1) is formed by the mixture of four interband transitions as indicated by the red arrows in (a). In the inset in (b), the squared electron amplitude [$n = |\Phi_S(r_e, r_h = 0)|^2$ in arbitrary units (a.u.)] of the I_1 exciton on a cross-sectional tubular plane with the hole fixed at the position of the red sphere (see text) is displayed. Si and C atoms are represented by cyan and yellow spheres, respectively.

exciton formation can become prominent in the optical spectra of SiC-NTs. To study excitonic effects on the optical properties of SiC-NTs, we have performed GW + BSE calculations by taking into account the electron-hole interaction kernel for several SiC-NTs of different sizes and different chiralities.

In Fig. 7, the quasiparticle band structure and the imaginary part of the optical polarizability for the ultrasmall armchair

(3,3) SiC-NT are presented. Because of the strong depolarization effects in NTs,[50] only the optical response for light polarized along the tube axis is significant. Therefore, only this polarization is considered here. For comparison, the optical absorption spectrum obtained without the electron-hole interaction in the GW + RPA scheme is also displayed in Fig. 7 [dashed (blue) curve in Fig. 7(b)]. The onset energy (4.86 eV) of this independent-particle optical spectrum corresponds to the lowest energy dipole-allowed vertical transition (E^{I_1}) from the valence to the conduction bands near two-thirds of the Γ-Z line in the Brillouin zone, which corresponds to the K point in the hexagonal Brillouin zone of the SiC sheet [see Fig. 7(a)].

When the interaction between electrons and holes is included, excitons with specific excitation energies (Ω) are formed, to give rise to prominent photoabsorption peaks. The binding energy of the lowest energy exciton is defined as the energy difference between the continuum onset and the corresponding excitation energy. For the armchair (3,3) SiC-NT, the optical absorption spectrum from GW + BSE calculations is dominated by discrete exciton peaks [see the red curves in Fig. 7(b)]. The first bright exciton (I_1), appearing at 2.86 eV with the high binding energy ($E_B^{I_1}$) of ~2.0 eV, is formed by a mixture of four pairs of interband transitions, as indicated by the arrows in Fig. 7(a). These four different interband transitions couple strongly, to make the electron amplitude more localized and highly asymmetric around the hole position located outside the tube but near the C atom, as displayed in the inset in Fig. 7(b), thereby resulting in the strongly bound character of exciton I_1. At the same time, the large electron-hole overlap in the (3,3) SiC-NT lifts the double degeneracy of the $E_1^{\pi-\pi*}$ exciton in the 2D SiC sheet to create the bright I_1 exciton and a dark exciton with a higher (by 0.02 eV) excitation energy. Similar excitonic effects are also found in the larger armchair (5,5) SiC-NT (see Table II). However, the lowest optically active exciton in the (5,5) SiC-NT has the lower binding energy of $E_B^{I_1} = 1.42$ eV, because of the reduced electron-hole overlap due to the

TABLE II. Binding energies (E_B) of the first bright exciton (I_1) and lowest energy dark exciton (K_1) below I_1 for the single-wall zigzag and armchair SiC nanotubes (NTs) considered here. The exciton binding energy (E_B) is calculated as the energy difference between the onset energy (E) of the corresponding interband transition continuum and the excitation energy (Ω). The tube diameter (D) and quasiparticle energy gap (E_{gap}^{QP}) are listed for comparison. The symbol (i) denotes an indirect band gap in armchair SiC-NTs. Moreover, the results for the SiC sheet, which can be considered the limiting case of an infinite-diameter SiC-NT, are also listed for comparison. All energies are in units of electron volts.

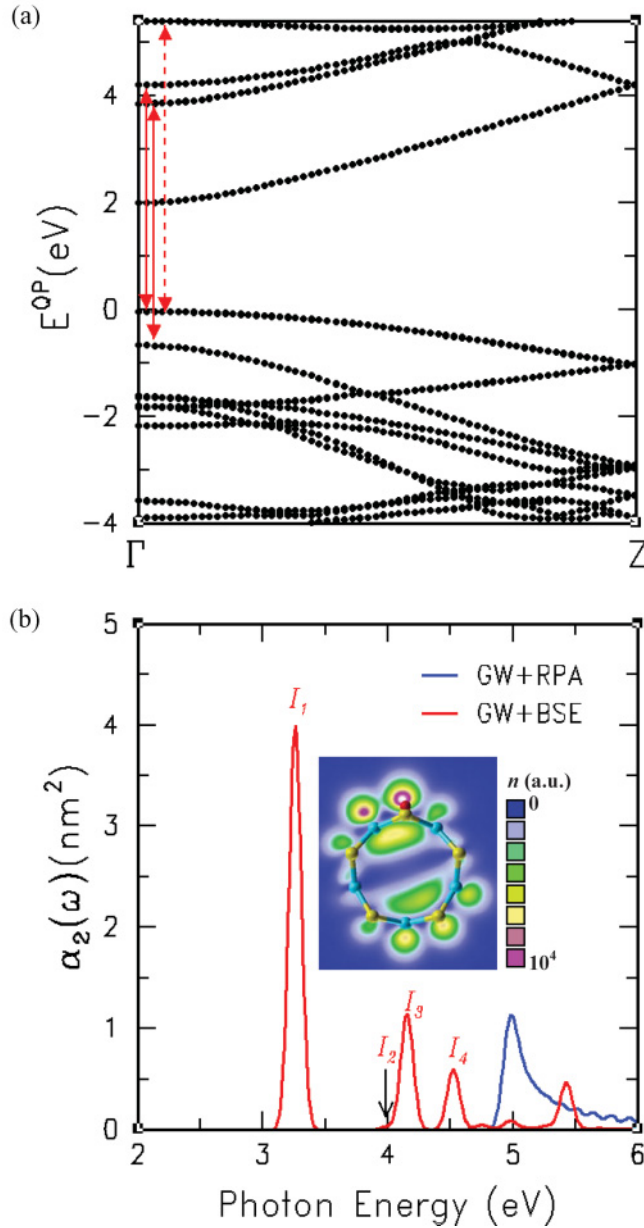|	D (Å)	E_{gap}^{QP}	E^{K_1}	E^{I_1}	Ω^{K_1}	Ω^{I_1}	$E_B^{K_1}$	$E_B^{I_1}$
NT								
(3,3)	5.05	4.09(i)		4.86		2.86		2.00
(4,4)	7.43	3.81(i)		4.75		3.12		1.63
(5,5)	8.45	4.15(i)		4.55		3.13		1.42
(5,0)	5.10	2.02	2.02	4.92	0.28	3.21	1.64	1.71
(6,0)	6.06	2.51	2.51	5.70	0.95	4.24	1.56	1.46
Sheet	∞	4.42		4.42		3.25		1.17

FIG. 8. (Color online) (a) Quasiparticle band structure and (b) optical absorption spectrum (broadened with a Gaussian width of 0.15 eV) of the zigzag (5,0) SiC-NT. In (b), the first bright exciton, I_1, is mainly related to the interband transition indicated as the solid (red) arrow in (a), whereas the transition by the dashed (red) arrow in (a) corresponds to the third (I_3) bright exciton in (b). The inset in (b) shows the squared electron amplitude (n, in arbitrary units) of I_1 with the fixed hole position marked by the red sphere. Si and C atoms are represented by cyan and yellow spheres, respectively.

decreased curvature. Moreover, apart from the bright bound and resonant excitons shown as red peaks in Fig. 7(b), there also exist many dark excitons among the bright ones. However, we find no dark exciton below the I_1 exciton in the armchair SiC-NT. As mentioned before, this could be anticipated from the fact that the isolated SiC layer has a direct band gap at the K point. In this case, there is no momentum mismatch when

the SiC sheet is rolled up to form an armchair SiC-NT, and hence the possibility of the formation of the optically inactive lowest energy exciton diminishes.[45]

Next let us concentrate on the excitonic effects on optical absorption in small-radius zigzag SiC-NTs. In order to scrutinize the chirality effects, we performed GW + RPA and GW + BSE calculations of the zigzag (5,0) SiC-NT with a tube radius comparable to that of the armchair (3,3) SiC-NT. The quasiparticle band structure and optical polarizability α_2 of the (5,0) SiC-NT is displayed in Figs. 8(a) and 8(b), respectively. In Fig. 8(b), label I_j denotes the jth optically allowed excited state. The inset in Fig. 8(b) is a contour plot of the electron charge density distribution of the I_1 exciton with respect to a fixed hole position. Like the (3,3) SiC-NT, the photoexcited spectrum of the (5,0) SiC-NT is characterized by discrete exciton peaks. The first bright exciton I_1 is the most prominent feature in the spectrum, and consists of the different interband transitions near the zone-center Γ point (represented by the solid arrow). As a result, the charge density distribution is not cylindrically symmetric. Similar results are found in the (6,0) SiC-NT, and the corresponding excitation energies are listed in Table II. Interestingly, although the (5,0) and (3,3) SiC-NTs have a similar curvature, the relatively lower binding energy (0.3 eV) of the I_1 exciton in the (5,0) SiC-NT indicates a rather delocalized exciton. This pronounced chirality effect can be attributed to the considerable orbital rehybridization in the zigzag SiC-NTs emphaszied above. This orbital rehybridization induces a significant band-gap reduction giving rise to the increased effective screening and, hence, reduces the binding energy. Furthermore, according to the zone-folding scheme for NTs, the lowest energy optically active interband transition at the K point of the 2D sheet can be folded into the Γ point to form a bright exciton with the lowest excitation energy in zigzag NTs. However, in very-small-radius zigzag SiC-NTs such as the (5,0) NT, the strong curvature-induced orbital rehybridization has brought a higher conduction band down to the GW band gap (0.0- to 0.4-eV) region [see Fig. 8(a)]. Since the optical transitions from the top valence bands to this conduction band are dipole-forbidden, some low-energy dark excitons, including the K_1 dark exciton, appear in the small-radius zigzag SiC-NTs. As reported in Table II, this low-energy K_1 dark exciton is also rather localized with a high binding energy, and this could make the zigzag SiC-NTs candidates for the tunable optical devices for temperature or external field sensors.

Finally, we explore the extent of the exciton wave function localization in the different SiC-NTs by comparing the intensity of their electron-hole wave functions in real space. In Fig. 9, isosurface plots of the electron density with the fixed hole position [(red) "X"] of the first bright exciton (I_1) of the armchair SiC-NTs suggest a significant local distribution in the direction along the circumference of the tube. Mixing of excitations to different sub-band pairs in small-radius SiC-NTs is responsible for this tightly bound character. In addition, a spatial localization of the exciton wave function along the tubular direction is also revealed by integrating out the electron coordinates in the perpendicular plane (red curves). In contrast to CNTs, the deviation from the 1D nature of the
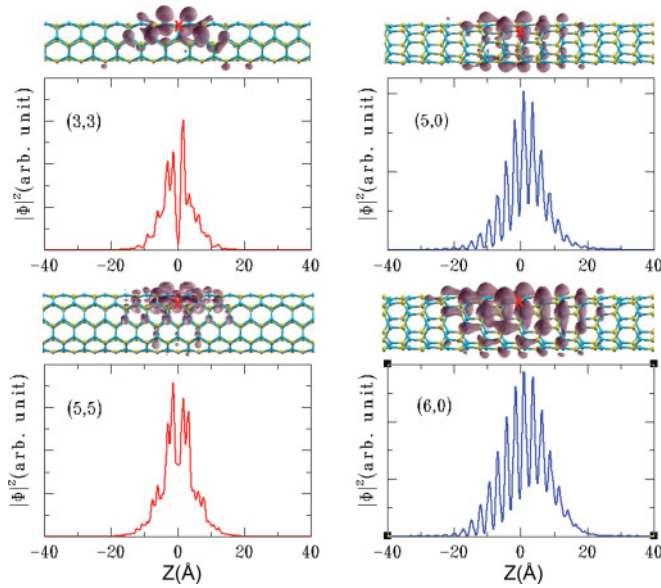
FIG. 9. (Color online) Isosurface plots of the electron distribution $|\Phi|^2$ of the I_1 exciton (see Figs. 7 and 8) with the fixed hole position [indicated by the (red) "X"] in the armchair (3,3) and (5,5) as well as the zigzag (5,0) and (6,0) SiC-NTs. The corresponding integrated intensities, obtained by averaging out the coordinates perpendicular to the tube axis, are also shown. Here the hole position is set at 0. Si and C atoms are represented by cyan and yellow spheres, respectively.

low-energy exciton is mainly attributed to the strong mixing of the interband transitions. Similar tightly bound behavior of the lowest-energy bright exciton has also been discovered in BN-NTs.[24] In zigzag SiC-NTs, we find a similar anisotropic bound nature of the first bright exciton. The slightly broadened distribution of the integrated wave-function intensity (see blue curves in Fig. 9) suggests a less bound character in zigzag SiC-NTs. The distinct spiky features in the curve are located on the cation (Si atom) planes and they indicate a charge transfer from an anion (hole) to its neighboring cations by photoexcitation. On the other hand, pronounced peak structures are not observed in the armchair SiC-NT because of the specific atomic arrangement dictated by its particular chirality. Furthermore, the asymmetric distribution of $|\Phi|^2$ with respect to the fixed hole position is a consequence of the different nearest-neighbor cation-anion distances caused by rolling up the ideal symmetric 2D SiC sheet. This curvature-induced spatial symmetry breaking is also responsible for the special nodal-like feature near the hole position in the smallest armchair (3,3) SiC-NT. Nonetheless, by comparing the distribution of the exciton wave function of the (3,3) SiC-NT with that of the larger (5,5) NT, we note that this symmetry breaking will decrease gradually as the curvature decreases or the tube diameter increases.

VI. CONCLUSIONS

In summary, we have employed state-of-the art many-body GW and GW + BSE approaches to study the quasiparticle band structure and optical properties, respectively, of a SiC sheet and related SiC NTs. First, we find a direct quasiparticle band gap for the isolated 2D SiC sheet. Our GW band structure calculations show that rather complicated orbital-dependent self-energy corrections are needed in obtaining accurate quasiparticle properties for an isolated SiC layer. The profile of the optical spectra is modified dramatically when the electron-hole interaction is included. In particular, a strongly bright bound exciton with a high binding energy (1.17 eV) is found to dominate the optical spectrum, because of the enhanced overlap between the electron and the hole orbitals due to reduced-dimensionality effects and also the existence of a vacuum region which reduces the effective screening in the SiC sheet.

Second, the quasiparticle band structure of small-radius armchair and zigzag SiC-NTs is systematically studied within the GW approximation. Our detailed analysis of the charge density distributions reveals that a curvate-induced orbital rehybridization plays a vital role in determining the band gap of small-radius SiC-NTs with different chiralities at both the LDA and the GW levels. In particular, quasiparticle band gaps as a function of tube diameter behave very differently, depending on the chirality of the SiC-NTs concerned.

Finally, the calculated photoexcited spectra consist of discrete exciton peaks, thereby indicating strong excitonic effects in both armchair and zigzag SiC-NTs. Optical absorption spectra of small-radius armchair and zigzag SiC-NTs are dominated by the first bright bound exciton, I_1, with a significant binding energy, up to ∼2.0 eV. The highly asymmetric charge distribution of exciton I_1 in the (3,3) SiC-NT is found to be a consequence of the strong coupling of the four optically allowed inter-sub-band transitions. Interestingly, we also find a quasi-0D bound character of the first bright exciton in SiC-NTs, and curvature-induced symmetry breaking affects the shape and size of this bound exciton. Moreover, our GW and BSE calculations demonstrate that the simple zone-folding approach fails in predicting low-energy exciton characters in very small zigzag SiC-NTs, mainly because of the strong curvature-induced orbital rehybridization in these NTs. We believe that the high excitation energy of ∼3.0 eV of the first bright exciton, with no dark exciton below it, may make small-radius armchair SiC-NTs candidates for optical devices working in the UV regime. In contrast, the numerous dark excitons below I_1 in zigzag SiC-NTs may lead to potential applications in tunable optoelectric devices ranging from IR to UV frequencies by external perturbations.

*hchsueh@mail.tku.edu.tw

†gyguo@phys.ntu.edu.tw

[1] K. H. Hellwege and O. Madelung (eds.), *Semiconductors: Physics of Group IV Elements and III–V Compounds*, Landolt-Börnstein, New Series, Groups IV and III–V, Pt. A (Springer-Verlag, Berlin, 1982), Vol. 17.

[2] R. W. G. Wyckoff, *Crystal Structures* (Wiley, New York, 1963).

[3] P. A. Ivanov and V. E. Chelnokov, Semicond. Sci. Technol. **7**, 863 (1992).

[4] C. Persson and U. Lindefelt, J. Appl. Phys. **82**, 5496 (1997).

[5] R. Wang, D. Zhang, and C. Liu, Chem. Phys. Lett. **411**, 333 (2005).

[6] R. Rurali, P. Godigonon, J. Rebollo, E. Hernandez, and P. Ordejon, Appl. Phys. Lett. **82**, 4298 (2003).

[7] C. H. Park, B. H. Cheong, K. H. Lee, and K. J. Chang, Phys. Rev. B **49**, 4485 (1994)

[8] G. L. Harris (ed.), *Properties of Silicon Carbide* (INSPEC, Institution of Electrical Engineers, London, 1995).

[9] X.-H. Sun, C.-P. Li, W.-K. Wong, N.-B. Wong, C.-S. Lee, S.-T. Lee, and B.-K. Teo, J. Am. Chem. Soc. **124**, 14464 (2002).

[10] S. Iijima, Nature (London) **354**, 56 (1991).

[11] R. Saito, G. Dresselhaus, and M. S. Dresselhaus, *Physical Properties of Carbon Nanotubes* (Imperial College Press, London, 1998).

[12] G. Y. Guo, K. C. Chu, D. S. Wang, and C. G. Duan, Phys. Rev. B **69**, 205416 (2004).

[13] A. Rubio, J. L. Corkill, and M. L. Cohen, Phys. Rev. B **49**, 5081 (1994).

[14] G. Y. Guo and J. C. Lin, Phys. Rev. B **71**, 165402 (2005).

[15] M. Zhao, Y. Y. Xia, D. J. Zhang, and L. M. Mei, Phys. Rev. B **68**, 235415 (2003).

[16] S. M. Lee, Y. H. Lee, Y. G. Hwang, J. Elsner, D. Porezag, and Th. Frauenheim, Phys. Rev. B **60**, 7788 (1999).

[17] I. J. Wu and G. Y. Guo, Phys. Rev. B **76**, 035343 (2007).

[18] I. J. Wu and G. Y. Guo, Phys. Rev. B **78**, 035447 (2008).

[19] Y. Miyamoto and B. D. Yu, Appl. Phys. Lett. **80**, 586 (2002).

[20] M. Menon, E. Richter, A. Mavrandonakis, G. Froudakis, and A. N. Andriotis, Phys. Rev. B **69**, 115322 (2004).

[21] G. Y. Guo and J. C. Lin, Phys. Rev. B **72**, 075416 (2005); **77**, 049901(E) (2008).

[22] G. Y. Guo, S. Ishibashi, T. Tamura, and K. Terakura, Phys. Rev. B **75**, 245403 (2007).

[23] C. D. Spataru, S. Ismail-Beigi, L. X. Benedict, and S. G. Louie, Phys. Rev. Lett. **92**, 077402 (2004).

[24] C.-H. Park and C. D. Spataru, and S. G. Louie, Phys. Rev. Lett. **96**, 126105 (2006).

[25] K. S. Novoselov, A. K. Geim, S. V. Morozov, D. Jiang, Y. Zhang, S. V. Dubonos, I. V. Grigorieva, and A. A. Firsov, Science **306**, 666 (2004).

[26] A. H. Castro Neto, F. Guinea, N. M. R. Peres, K. S. Novoselov, and A. K. Geim, Rev. Mod. Phys. **81**, 109 (2009).

[27] M. Rohlfing and S. G. Louie, Phys. Rev. Lett. **81**, 2312 (1998).

[28] M. Rohlfing and S. G. Louie, Phys. Rev. B **62**, 4927 (2000).

[29] W. Kohn and L. J. Sham, Phys. Rev. **140**, A1133 (1965).

[30] M. S. Hybertsen and S. G. Louie, Phys. Rev. Lett. **55**, 1418 (1985).

[31] M. S. Hybertsen and S. G. Louie, Phys. Rev. B **34**, 5390 (1986).

[32] B. G. Pfrommer, M. Cote, S. G. Louie, and M. L. Cohen, J. Comput. Phys. **131**, 233 (1997).

[33] L. Kleinman and D. M. Bylander, Phys. Rev. Lett. **48**, 1425 (1982).

[34] H. J. Monkhorst and J. D. Pack, Phys. Rev. B **13**, 5188 (1976).

[35] L. Hedin, Phys. Rev. **139**, A796 (1965).

[36] W. G. Aulbur and L. Jonsson, and J. W. Wilkins, *Solid State Physics: Advances in Research and Applications*, Vol. 54 (Academic, New York, 2000), p. 1.

[37] C. D. Spataru, S. Ismail-Beigi, R. B. Capaz, and S. G. Louie, *Carbon Nanotubes: Advanced Topics in the Synthesis, Structure, Properties and Applications* (Springer-Verlag, Heidelberg, 2008), Vol. 111 p. 195.

[38] J. B. Neaton, M. S. Hybertsen, and S. G. Louie, Phys. Rev. Lett. **97**, 216405 (2006).

[39] C. D. Spataru, S. Ismail-Beigi, L. X. Benedict, and S. G. Louie, Appl. Phys. A **78**, 1129 (2004).

[40] S. Ismail-Beigi, Phys. Rev. B **73**, 233103 (2006).

[41] L. Yang, J. Deslippe, C.-H. Park, M. L. Cohen, and S. G. Louie, Phys. Rev. Lett. **103**, 186802 (2009).

[42] H. Sahin, S. Cahangirov, M. Topsakal, E. Bekaroglu, E. Akturk, R. T. Senger, and S. Ciraci, Phys. Rev. B **80**, 155453 (2009).

[43] R. T. M. Ummels, P. A. Bobbert, and W. van Haeringen, Phys. Rev. B **58**, 6795 (1998).

[44] Here we also performed the LDA, GW, and BSE calculations for bulk 2H SiC and found the LDA and GW band gaps to be 2.10 and 3.17 eV, respectively. The BSE calculation predicts the exciton binding energy in 2H SiC to be 0.1 eV.

[45] S. Ismail-Beigi, Phys. Rev. B **77**, 035306 (2008).

[46] X. Blase, L. X. Benedict, E. L. Shirley, and Steven G. Louie, Phys. Rev. Lett. **72**, 1878 (1994).

[47] L. Yang, M. L. Cohen, and S. G. Louie, Nano Lett. **7**, 3112 (2007).

[48] E. R. Margine and V. H. Crespi, Phys. Rev. Lett. **96**, 196803 (2006).

[49] J. Deslippe, M. Dipoppa, D. Prendergast, M. V. O. Moutinho, R. B. Capaz, and S. G. Louie, Nano Lett. **9**, 1330 (2009).

[50] H. Ajiki and T. Ando, Physica (Amsterdam) B **201**, 349 (1994).